Supplementary Information

Tailoring zinc-ion deep eutectic electrolytes through dual regulation of solvation shell volume and solvent polarity

Mingming Han [a], Yongxing Ding [a, b], Jing Lou [c], Jia Wang [b], Minghan Yang [b], Lutong Shan [b, d, *], Chao Qiu [b, *], Zhenyue Xing [b], Zaowen Zhao [b], Xiaodong Shi [b, *]

[a] Hangzhou Institute of Advanced Studies, Zhejiang Normal University, Hangzhou 311231, China

[b] State Key Laboratory of Tropic Ocean Engineering Materials and Materials Evaluation, School of Marine Technology and Equipment, School of Materials Science and Engineering, Hainan University, Haikou 570228, China

[c] China Mobile (Hangzhou) Information Technology Co., Ltd. Hangzhou 311100, China

[d] Department of Chemical and Biomolecular Engineering, National University of Singapore, 117585, Singapore

* Corresponding authors emails: lutong_shan@nus.edu.sg; chaoqiu@hainanu.edu.cn; shixiaodong@hainanu.edu.cn

1. Experimental Section

1.1 Sample preparation

$Zn(BF_4)_2 \cdot xH_2O$ (95%), acetonitrile (AN, 99.5%) were purchased from Macklin company. Acetamide (Ace, >99%), dimethyl sulfoxide (DMSO, >99%), dimethyl carbonate (DMC, 99%), dimethyl sulfoxide-d6 (DMSO-d_6, ≥99.5 atom% D), deuterium oxide (D_2O, ≥99 atom% D), ultrahigh capacitance porous carbon activated carbon (AC), polyvinylidene fluoride, n-methyl-2-pyrrolidinone (electronic grade, >99.9%) were purchased from Aladdin company. Propylene carbonate (PC, 98%) was purchased from Kaiwei Chemical Manufacturer. Ethyl methyl carbonate (EMC, 99.9%), 1,3-dioxolane (DOL, 99.955%), ethylene carbonate (EC, 99.9%), dimethyl carbonate (DMC, > 99%) were purchased from Duoduo Co., Ltd. Super P was sourced from Guangdong Canrd New Energy Technology Co., Ltd. All chemical reagents were used as received unless otherwise stated.

The DES was prepared as follows: the mixture of $Zn(BF_4)_2 \cdot xH_2O$ and acetamide with the molar ratios of 1:7 was heated at 70°C to obtain the liquids, and then cooled back to room temperature with being kept for 12 hours before usage. The DES-AN, DES-H_2O and DES-DMSO were prepared through introducing the additives of AN, H_2O and DMSO into the DES with the volume ratio of 10%. Active carbon (AC)-I_2 composite material (weight ratio=1:3) was synthesized through facile gas-adsorption method at 80°C for 6 hours under vacuum as reported in previous works. Corresponding cathodes were prepared by casting slurries mixed with AC-I_2 composite (70 wt.%), Super P (20 wt.%), polyvinylidene fluoride (10 wt.%) and n-methyl-2-pyrrolidinone solvent onto the carbon paper current collector (1.13 cm^2), which were dried at 40 °C for 24 hours under vacuum. The mass loading of active material was about 0.8 mg.

1.2 Material characterization

Raman spectra were conducted on a spectrophotometer (DXR, Thermo-Fisher Scientific) with a wavelength of 532 nm. Fourier infrared spectroscopy (FTIR) spectra of electrolytes were recorded by FTIR

spectrometer (Shimadzu Corporation, IRTRACER-100). Samples were scanned from −150 °C-25°C at a rate of 5°C min^{-1} under a nitrogen atmosphere to evaluate their thermal properties using a differential scanning calorimeter (DSC). The Zn K-edge X-ray absorption fine structure (XAFS) measurements were performed at a beamline of the Shanghai Synchrotron Radiation Facility using the easyXAFS system in transmission mode under operating conditions of 30 kV and 3 mA. ^{1}H nuclear magnetic resonance (^{1}H NMR) and pulsed-field-gradient NMR (PFG-NMR) were recorded at 600 MHz NMR (Bruker, Avance NEO 600), while ^{1}H-^{1}H correlation spectroscopy NMR (^{1}H-^{1}H COSY) were recorded at 400 MHz NMR (Bruker, Avance NEO 400). ^{1}H NMR sample preparation employs DMSO-d_6 as the deuterated solvent, thereby avoiding interference from proton exchange in protic solvents affecting the NH_2 group. For both ^{1}H-^{1}H COSY and PFG-NMR measurements, D_2O was used as the deuterated solvent. Specifically, for the ^{1}H-^{1}H COSY experiment, the sample was sealed in a capillary tube (serving as the inner tube), which was then placed within an outer tube containing D_2O. The morphologies of Zn electrode were analyzed by FEI Nova NanoSEM 230 machine. Transmission electron microscopy/high-resolution transmission electron microscopy (TEM/HR-TEM) characterizations were carried on Titan G2 60-300 machine. The surface chemical composition information and evolution of Zn deposition were studied with XPS technique on an ESCALAB 250Xi X-ray photoelectron spectrometer (Thermo Fisher). The exploration on 3D height of Zn electrodes was operated on a commercial atomic force microscope (AFM, Bruker Dimension Icon) at room temperature.

1.3 Electrochemical tests

Electrochemical properties of Zn//Zn symmetric cells, Zn//Cu asymmetric cells, Zn//AC-I_2 full cells were tested using CR 2032 coin-type cells with the LAND testing system. Zn foils (80 μm thick, ~84 mg) were used as both the anode and cathode in Zn//Zn symmetric cells. Zn//Cu asymmetric cells were assembled using Zn anode and Cu cathode. The amount of electrolyte was 60 μl in Zn//Zn and Zn//Cu cells, 120 μl in Zn//AC-I_2 full cells, and 600 μl in Zn//AC-I_2 soft pack. Electrochemical impedance spectroscopy (EIS) and cyclic

voltammetry (CV) data were carried out on the electrochemical workstation (CHI660E, China). Chronoamperograms measurements and Tafel fit system were conducted in Zn//Zn symmetric cells in electrochemical workstation (CHI660E, China). The Zn^{2+} transference number (t_{Zn}^{2+}) tests were conducted in Zn//Zn symmetric cells in an AutoLab (PGSTAT302N, Switzerland) electrochemical workstation. In situ EIS tests were performed in a Gamry (Interface 1010E, USA) electrochemical workstation.

The electrolyte resistance was acquired from the intercept of Nyquist plot and the ionic conductivity was calculated according to the following equation:

$$\sigma = GL/A = L/RA \tag{1}$$

where σ (S cm^{-1}) is the per unit conductivity, G (S) is conductance, R is the electrolyte resistance, L (cm) is interval distance (cm) between the two stainless steel electrodes, A (cm^2) is electrode area.

The water molecule diffusivity was measured using PFG-NMR with a stimulated echo pulse sequence. Data were acquired with 18 linearly incremented gradient steps for each targeted resonance peak and subsequently fitted using the Stejskal-Tanner equation[1]:

$$\frac{I}{I_0} = \exp - \left[D_i \gamma^2 g^2 \delta^2 \left(\Delta - \frac{5\delta}{8} - \frac{\tau_1 + \tau_2}{2} \right) \right] \tag{2}$$

where I is the intensity of the stimulated echo with different field gradient g, I_0 is the intensity when $g = 0$, D_i is the diffusion constants, γ is the gyromagnetic ratio, g is the gradient strength including a correction for the sin-bell shape factor, δ is the gradient pulse duration, Δ is the drift delay, τ_1 and τ_2 are the gradient recovery delays.

The average coulombic efficiency was calculated using aurbach's method[2, 3]. First, excess zinc capacity (2 mAh cm^{-2}) was deposited and subsequently stripped to a cutoff voltage of 0.5 V. Subsequently, the charging/discharging capacity of 1 mAh cm^{-2} was cycled 20 times at 1 mA cm^{-2}. Finally, the zinc capacity was stripped to a cutoff voltage of 0.5 V. Calculated by the following equation:

$$ACE = \frac{nQ_C + Q_S}{nQ_C + Q_T} \tag{3}$$

where, n is the number of cycles, Qc is the capacity of each cycle, Qs is the last stripped charge capacity and Q_T is the first charge capacity.

The Zn//Zn cells were assembled and a small polarization potential (ΔV) at 10 mV was applied. Then the initial (I^o) and steady-state (I^{ss}) polarization current values were recorded. Correspondingly, the initial and steady-state values of the resistances (R^o and R^{ss}) were examined via EISs before and after the potentiostatic polarization. The t_{Zn}^{2+} was calculated following the equation[4]:

$$t_{Zn}^{2+} = I^{ss}(\Delta V - I^o R^o) / I^o(\Delta V - I^{ss} R^{ss}) \tag{4}$$

The relationship between CV sweep speed and peak current follows the following formula:

$$i = av^b \tag{5}$$

where, a is a constant, b is interrelated with the storage mechanism, i and v refer to current and scan rate, respectively.

The distribution of relaxation times (DRT) method obtains the relaxation time distribution through deconvolution algorithm, and the electrochemical impedance is expressed as follows[5]:

$$Z(f) = R_0 + i2\pi f L_0 + R_p \int_0^\infty \frac{g(\tau)}{1 + i2\pi f\tau} d\tau \tag{6}$$

where R_0 is an ohmic resistance, f is the frequency, L_0 is an inductance, R_p is an polarization impedance, τ is the relaxation time, and $g(\tau)$ is a timescale distribution. The software used to analyze the EIS data was MATLAB-based DRTtools[6], which was computed by continuous function discretization technique combined with Tikhonov regularization, while credibility interval were obtained by Bayesian approach[7].

1.4 Computational details

Density Functional Theory (DFT) calculations were performed by using the CP2K package[8] mixed Gaussian and plane-wave scheme[9] and the Quickstep module[10]. The Perdew-Burke-Ernzerhof (PBE) exchange correlation functional[11], Goedecker-Teter-Hutter (GTH) pseudopotential[12], DZVP-MOLOPT-SR-GTH / TZVP-MOLOPT-SR-GTH / TZVP-MOLOPT-GTH basis sets were used to describe the system[10]. A

plane-wave energy cut-off and relative cut-off of 400 Ry and 55 Ry have been employed, respectively. The energy convergence criterion was set to 10^{-6} Hartree. The DFT-D3(BJ) level correction for dispersion interactions was applied[13]. Structural optimization was performed using the Limited Memory Broyden-Fletcher-Goldfarb-Shannon (LBFGS) optimizer, until the maximum force is below 0.00045 Ry/Bohr (0.011 eV/Å). The electrostatic potential was calculated and plotted through the software Multiwfn[14] and Visual Molecular Dynamics (VMD)[15], respectively. Reduced density gradient (RDG) was calculated and plotted with the help of the software Multiwfn[14]. The Gibbs free-energy diagrams were estimated under zero potential (U = 0) by the equation[16]:

$$\Delta G_H = \Delta E_H + \Delta ZPE - T\Delta S \quad (7)$$

during which ΔE_H is the energy change between the reactant and product obtained from DFT calculations, ΔZPE is the change of zero point energy and T and ΔS represents the temperature and change of entropy, respectively. T = 298.15 K was employed in this case.

The molecular dynamics (MD) simulations were conducted in GROMACS software.[17] Water molecules were simulated with SPC/E model. Parameter fitting was performed using the density functional theory (DFT) package Orca[18] under B3LYP exchange-correlation functional with Grimme's DFT-D3(BJ) empirical dispersion correction. The RESP2(0.5) [Non-bonded force field model with advanced restrained electrostatic potential charges (RESP2)] charge combining gas- and liquid-phase (implicit solvent, SMD model) charges were adopted for all molecules in this work calculated using Orca[18] and Multiwfn package[14].

The electrolyte system was initialized using the Packmol package[19]. For DES electrolyte, the MD box has a size of 5×5×5 nm^3 and include 50 Zn^{2+}, 100 BF_4^-, 350 acetamide and 370 water molecules. For DES-AN electrolyte, the MD box has a size of 5×5×5 nm^3 and include 50 Zn^{2+}, 100 BF_4^-, 38 acetonitrile, 350 acetamide and 370 water molecules. For DES-H_2O electrolyte, the MD box has a size of 5×5×5 nm^3 and include 50 Zn^{2+}, 100 BF_4^-, 350 acetamide and 510 water molecules. The MD simulation was firstly performed in the NVT ensemble at temperature (298 K) by using 2 fs time step for 1 ns. Then equilibrium simulation is

performed in the NPT ensemble at constant pressure (1 bar) and temperature (298 K) in a cubic box with periodic boundary conditions in all xyz Cartesian directions by using 2 fs time step for 2 ns. Finally, the production simulation is performed in the NVT ensemble at temperature (298 K) by using 2 fs time step for 10 ns. The coordination number of molecules of type i in the first solvation shell surrounding a single molecule of type j is calculated as:

$$N_i = 4\pi n_j \int_0^{R_M} g_{ij}(r) r^2 dr \tag{8}$$

in which RM is the distance of the first minimum following the first peak in the radial distribution function (RDF), and $gij(r)$is a standard approach for bulk liquid. All the visualizations of MD simulations are implemented by VMD software[15]. The mean square displacement (MSD) of the atom is calculated by the Einstein equation:

$$MSD \equiv \sum_i^n [(R_i(t) - R_0(t))^2] \tag{9}$$

where R is the atomic coordinates, N is total number of atoms, and t is the time. The diffusion constant (D) is the slope of MSD versus times with a factor of 1/2:

$$D = \frac{MSD}{2t} \tag{10}$$

Supplementary Figures and Captions

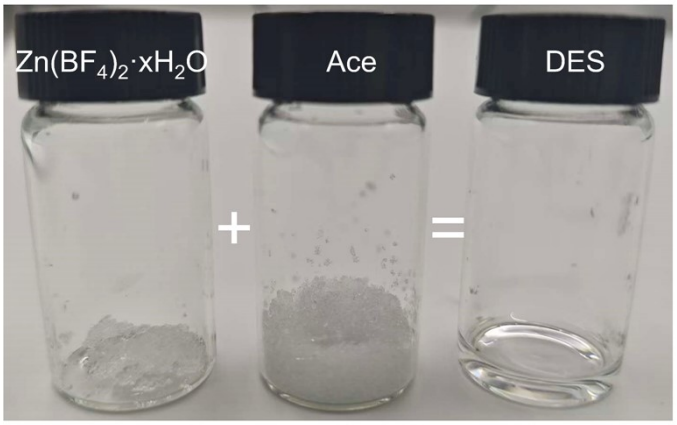

Figure S1 Preparation Process for Deep Eutectic Electrolyte.

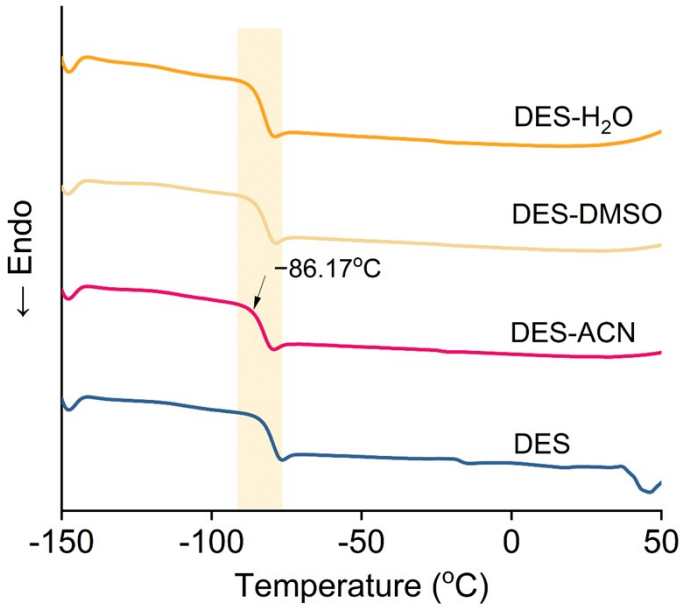

Figure S2 DSC data of different electrolyte systems.

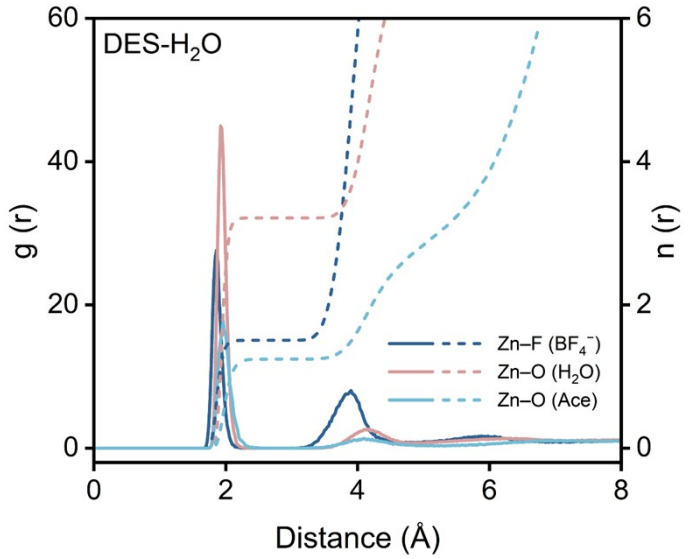

Figure S3 Radial distribution function (solid line, g(r)) and cumulative coordination number (dashed line, n(r)) for the DES-H_2O.

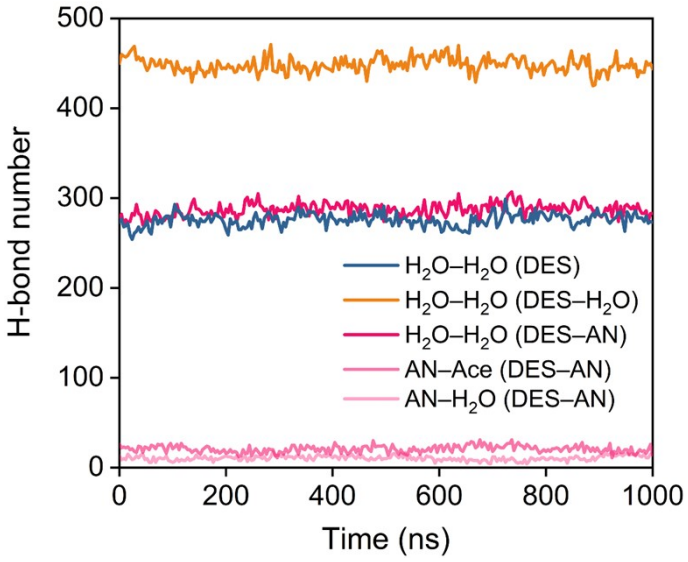

Figure S4 The number of H-bonds of different molecules.

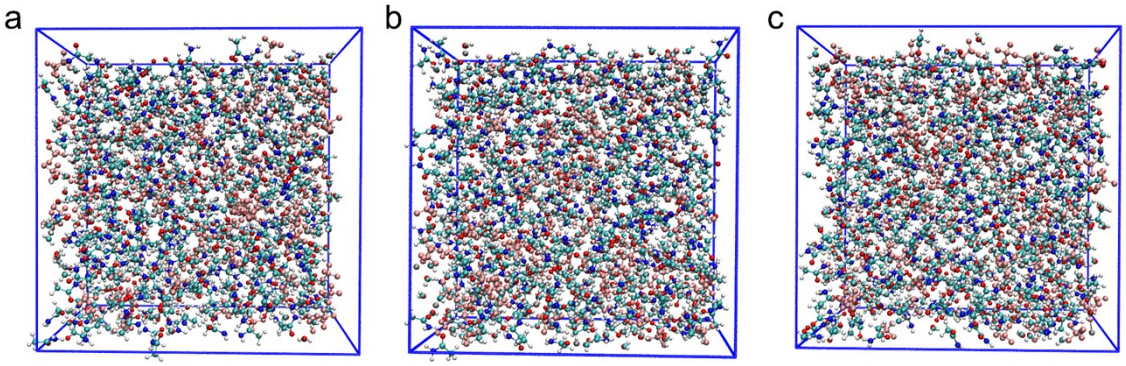

Figure S5 The MD snapshots of DES (a), DES-AN (b) and DES-H_2O (c).

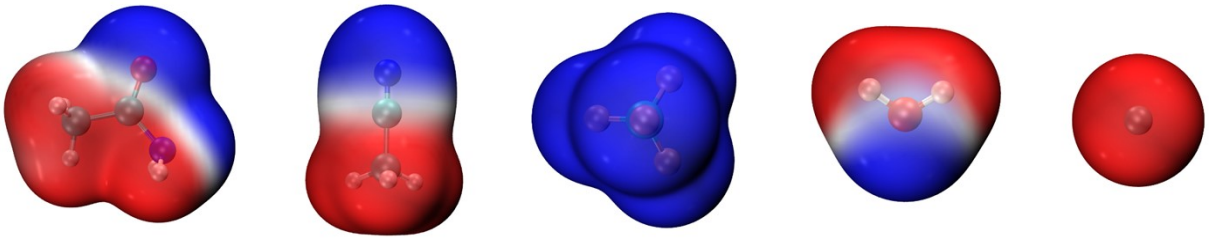

Figure S6 Electrostatic potential of different substances.

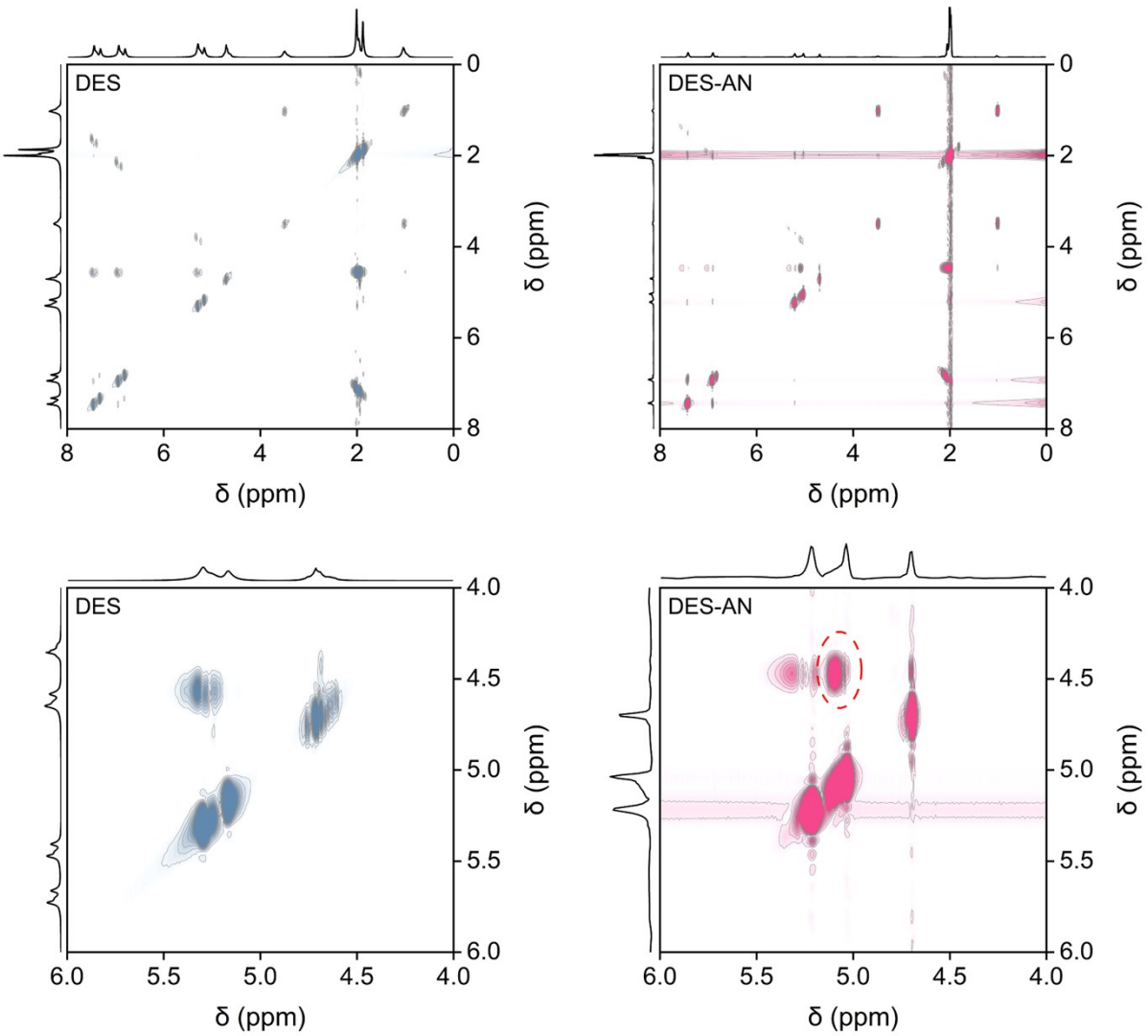

Figure S7 ^{1}H-^{1}H COSY NMR spectrum of DES and DES-AN in different ranges.

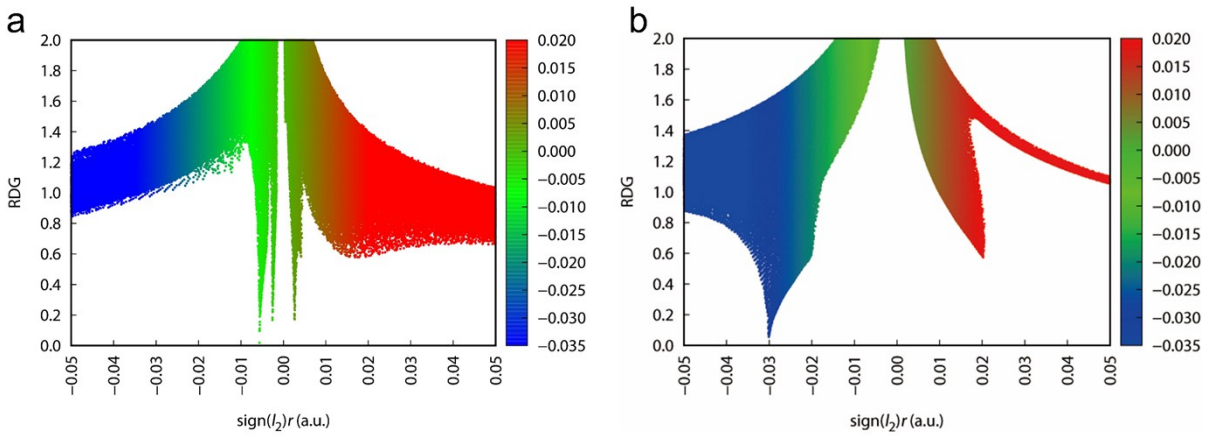

Figure S8 Gradient isosurfaces of (a) Ace–Ace and (i) H_2O–H_2O complexes obtained by the RDG method.

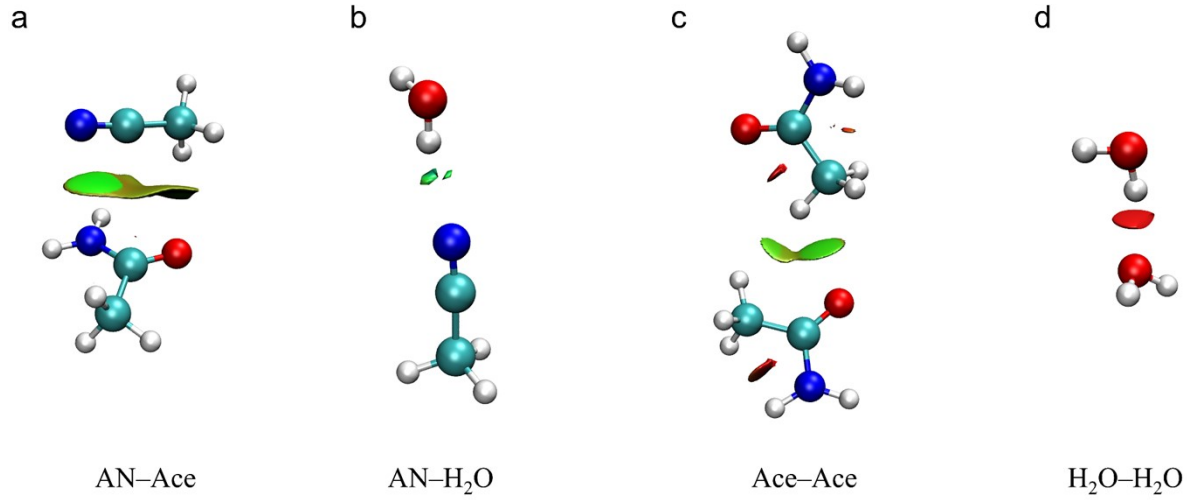

Figure S9 Schematic diagram of isosurfaces obtained by the RDG method for different complexes.

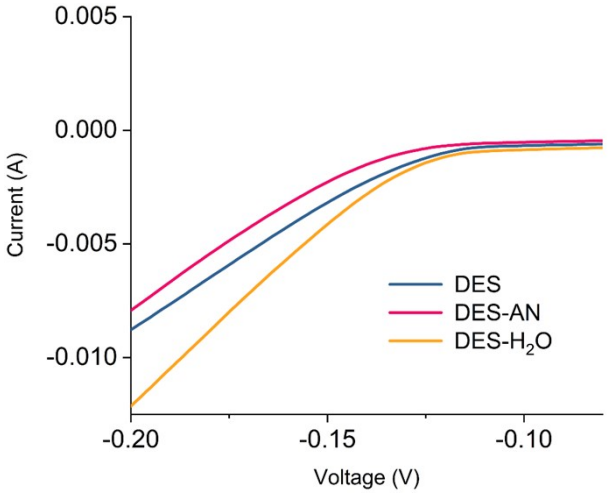

Figure S10 LSV curves of different electrolytes.

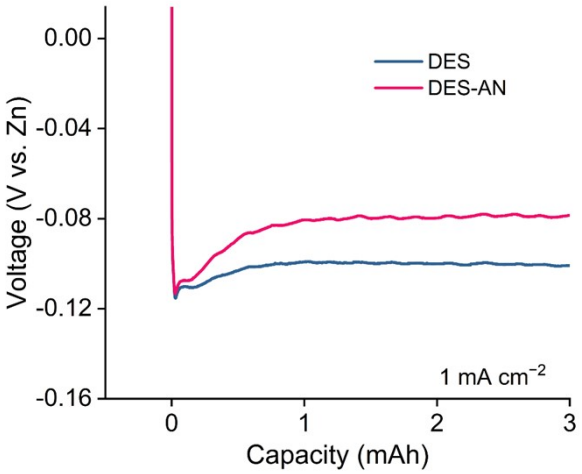

Figure S11 Nucleation overpotential of Zn on the Cu substrate in DES and DES-AN electrolytes

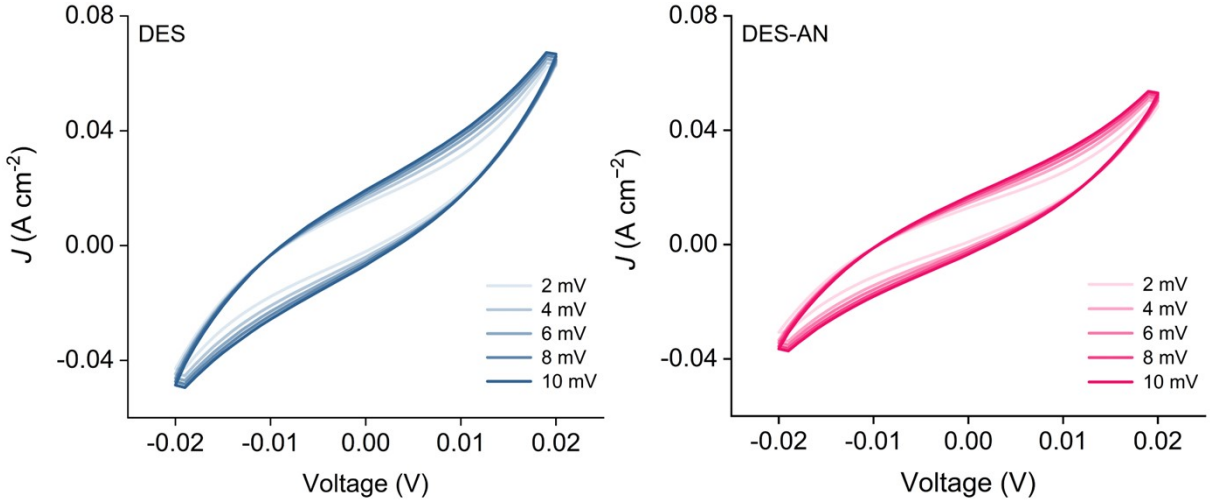

Figure S12 CV curves for the electric double-layer capacity measurement of Zn//Zn cells with (a) DES and (b) DES-AN in a voltage range of −20 to 20 mV under various scanning rates.

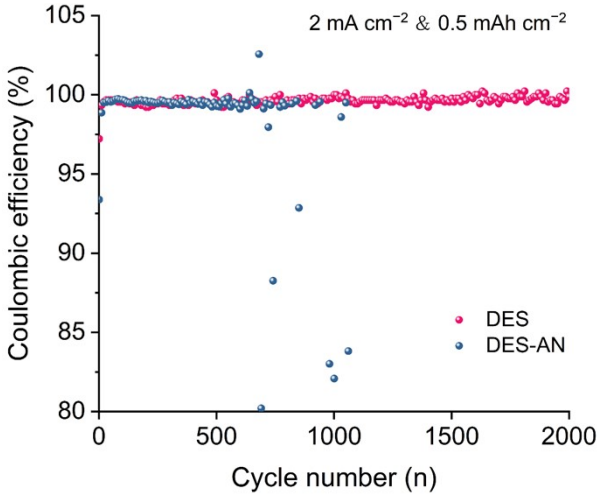

Figure S13 Coulombic efficiency tested in Zn//Cu cells in DES and DES-AN electrolytes.

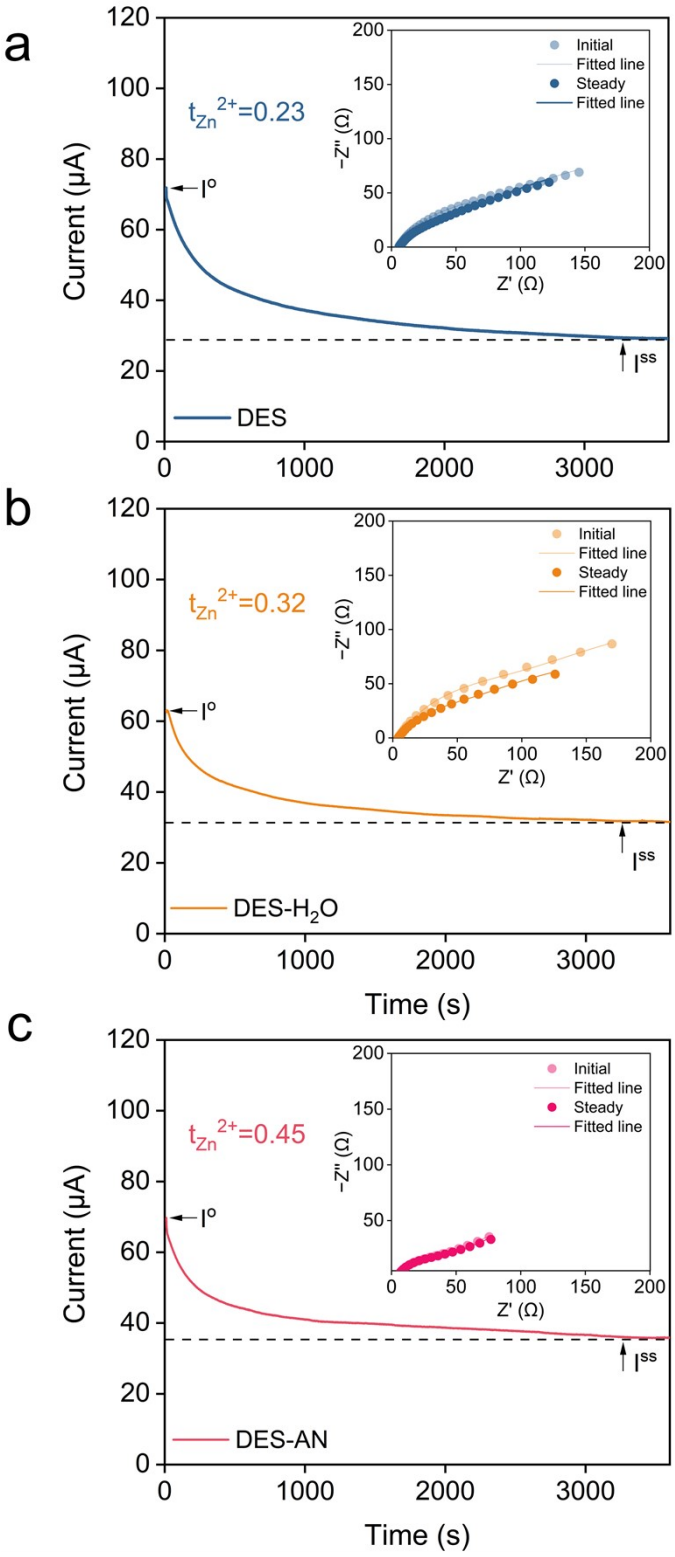

Figure S14 Zn^{2+} transference number (t_{Zn}^{2+}) of various electrolytes. The illustration shows the EIS before and after polarization.

Figure S15 XPS spectra of C 1s and N 1s of the zinc anodes after 10 cycles with DES, obtained after Ar^+ ion sputtering.

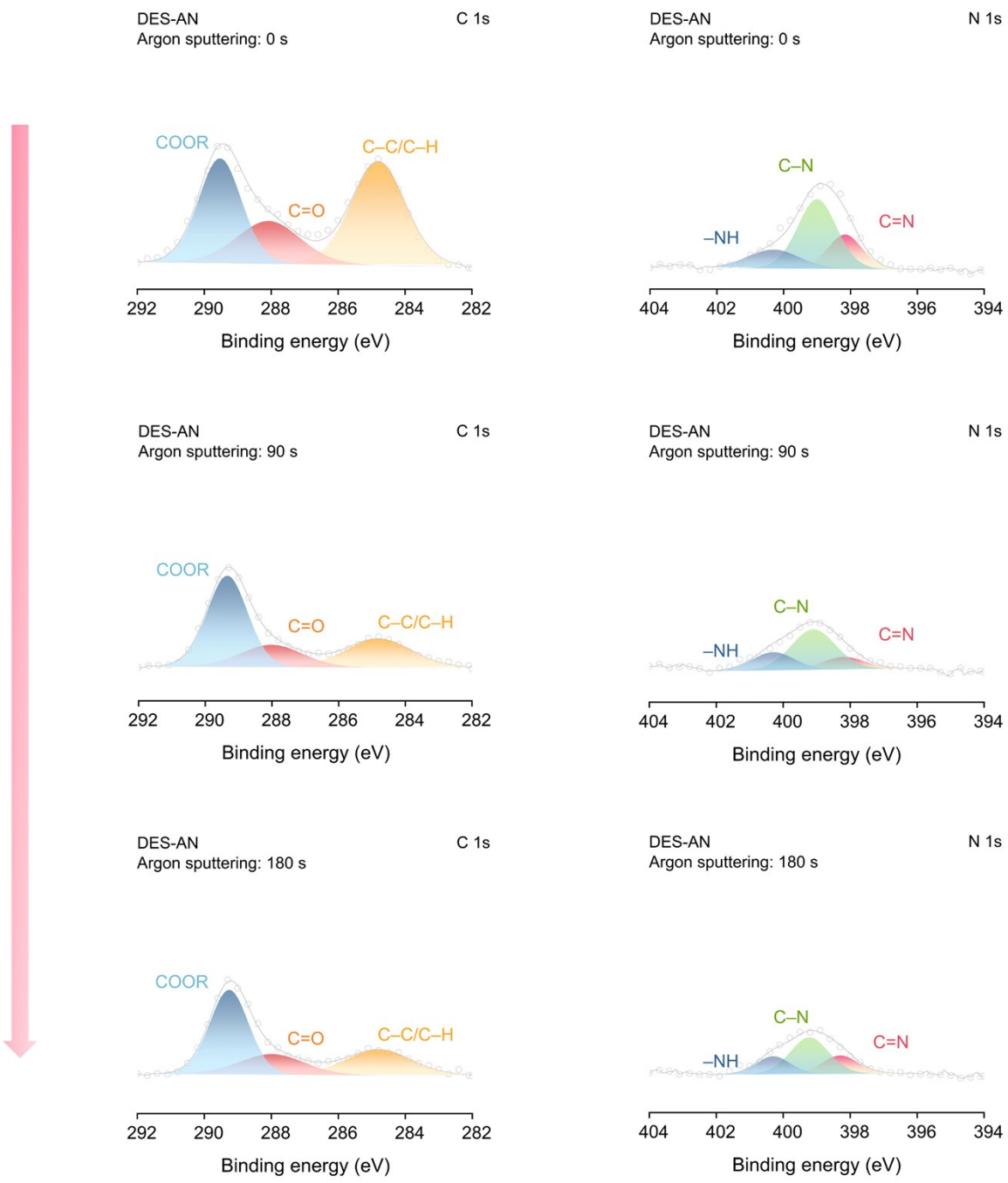

Figure S16 XPS spectra of C 1s and N 1s of the zinc anodes after 10 cycles with DES-AN, obtained after Ar^+ ion sputtering.

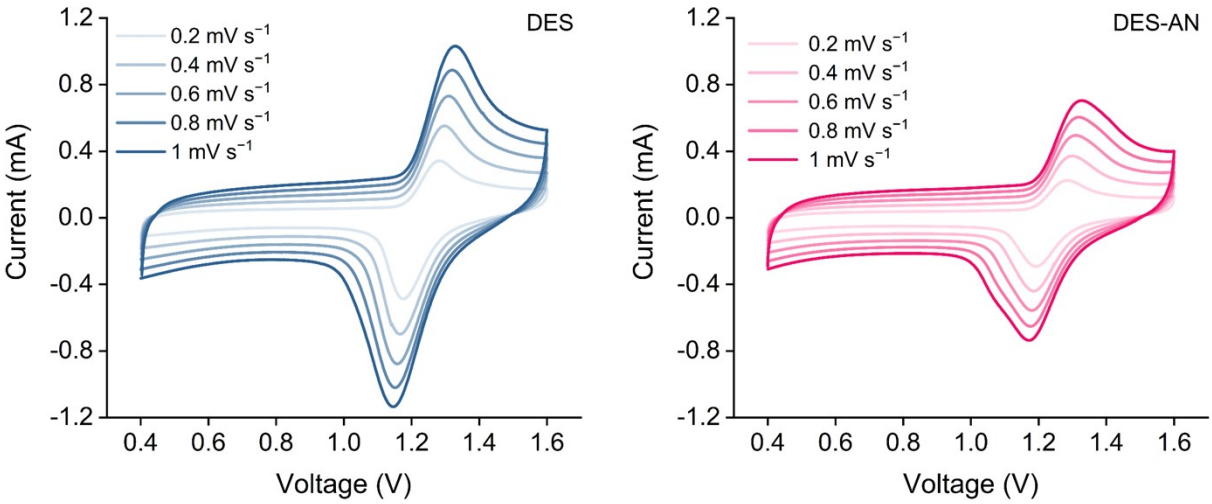

Figure S17 CV curves of ZIBs with (a) DES and (b) DES-AN at different scan rates.

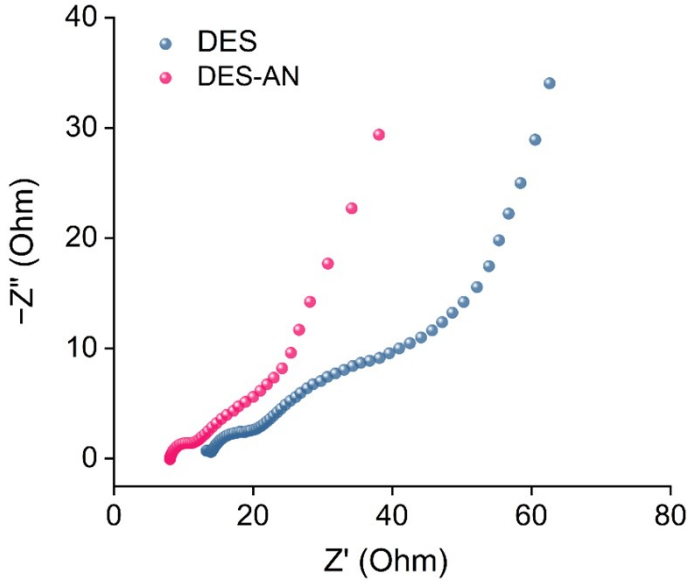

Figure S18 The EIS plots of ZIBs.

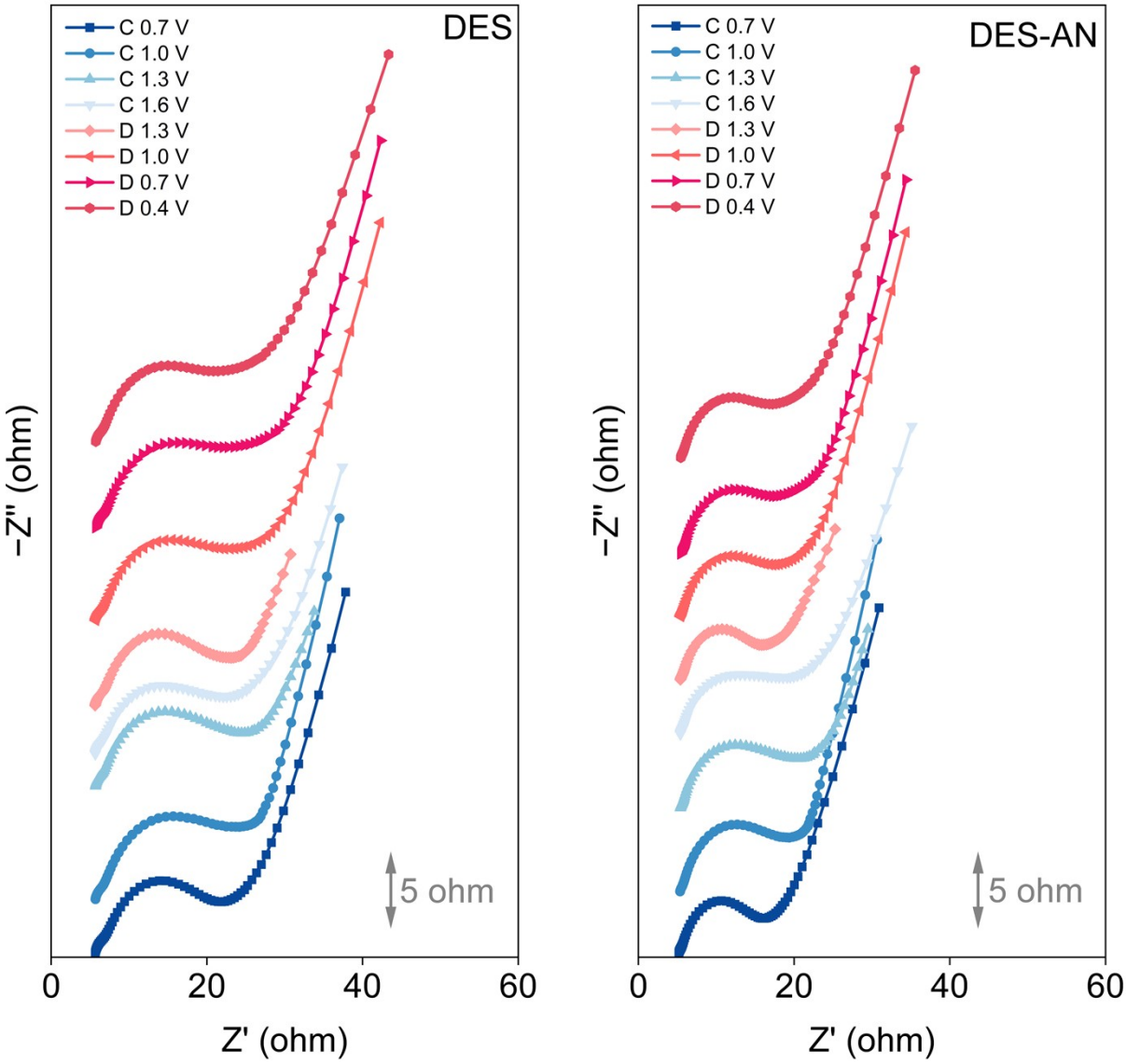

Figure S19 In situ EIS curves of ZIBs.

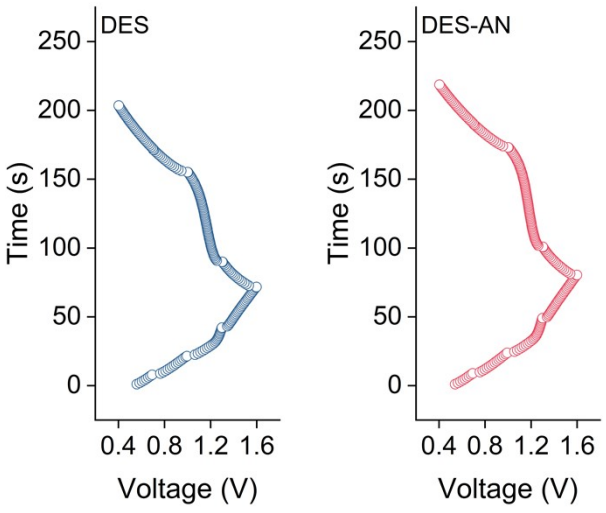

Figure S20 The voltage-time curve of in-situ EIS.

Table S1 ET(30), Solvation Energy, and Solvation Volume of Different Reagents

Reagent	Et(30)[20]	Solvation Energy (eV)	Solvation Volume (Å)
EMC (Ethyl methyl carbonate)	37.3	−21.8853	3669.1884
THF (tetrahydrofuran)	37.4	−41.2020	2465.8465
DMC (Dimethyl carbonate)	38.2	−21.3370	2795.0281
DME (1,2-Dimethoxyethane)	38.2	−3.13979	4228.9319
DOL (1,3-Dioxolane)	43.1	−7.0299	1469.3940
TMP (Trimethyl phosphate)	43.6	−28.7508	4745.8652
SL (Tetramethylene sulfone)	44.0	−54.7630	2359.2761
DMSO (Dimethyl sulfoxide)	45.1	−3.72089	1690.4745
AN (Acetonitrile)	45.6	−2.95845	1574.0524
PC (Propylene carbonate)	46.0	−12.7375	3785.4746
EC (Ethylene carbonate)	48.6	−12.6342	2506.4505
EG (Ethylene glycol)	56.3	−8.6014	2842.1685
H_2O (Water)	63.1	−0.98217	847.26217

Table S2 The binding energies of different ligands

Ligand	Binding Energy (eV)
SL	−10.2
TMP	−6.61
DOL	−4.73
EMC	−4.30
THF	−4.12
DMC	−3.90
EG	−3.17
PC	−1.94
EC	−1.67
DME	−1.49
DMSO	−1.27
AN	0.536
H_2O	2.80

Table S3 The ion conductivity of different electrolytes

Electrolyte	Conductivity (mS cm^{-1})
DES-EC	0.528
DES-PC	0.612
DES-DEC	1.44
DES-FEC	1.51
DES-DMC	1.58
DES	1.78
DES-EMC	2.39
DES-DMSO	5.37
DES-DOL	7.41
DES-AN	8.30
DES-H_2O	11.9

Table S4 Recent progress in Coulomb efficiency of the eutectic electrolytes

Electrolyte	mA cm^{-2}/ mAh cm^{-2}	Cycle number	Coloumbic efficiency	Ref.
$Zn(ClO_4)_2 \cdot 6H_2O$: sulfolane =1: 6(molar ratio)	0.5/0.5	100	98	Adv. Funct. Mater. (2021)[21]
$Zn(ClO_4)_2$ $6H_2O$: succinonitrile =1: 8 (molar ratio)	0.5/0.5	90	98.4	Joule (2020)[22]
$ZnCl_2$:acetamide:H_2O=1:3:1	0.1/0.025	1000	98	Adv. Funct. Mater. (2021)[23]
Ethylene glycol: zinc trifluorosulfonate: = 1:6 (molar ratio) + 30% H_2O (volume ratio)	1/0.5	1000	99.6	Energy Environ. Sci. (2023)[24]
$Zn(OAc)_2 \cdot 2H_2O$: $ZnCl_2$: H_2O: DOL=0.036: 0.054: 1: 0.162	1/1	1000	99.5	Angew. Chem. Int. Ed. (2023)[25]
LiTFSI: NMA=1: 4 (molar ratio) +10wt% FEC+ 3 wt% 2-(3-(6-methyl-4-oxo-1,4-dihydropyrimidin-2-yl)ureido)ethyl methacrylate+1.5 wt% pentaerythritol tetraacrylate+0.1 wt% 2,2′-azobis(2-methylpropionitrile)	0.2/0.4	100	99.2	Angew. Chem. Int. Ed. (2020)[26]
Acetamide: caprolactam=1:1(molar ratio)+50% H_2O+1 m zinc trifluorosulfonate	NA/NA	25	98.37	Adv. Mater. (2024)[27]
$Zn(Ac)_2$:Formamid=1:9 (molar ratio)	1/0.5	300	97.9	Angew. Chem. Int. Ed. (2024)[28]
$Zn(TFSI)_2$:Ace=1:7 (molar ratio)	0.5/1	10	98	Nat. Commun. (2019)[29]
1M $Zn(TFSI)_2$+ (Sulfolane:H_2O=2:1, molar ratio)	1/1	350	99.3	Angew. Chem. Int. Ed. (2023)[30]
propylene glycol:H_2O=5:1 (volume ratio) + 2 m $ZnSO_4 \cdot 7H_2O$	1/0.5	2000	99.3	Angew. Chem. Int. Ed. (2023)[31]

$Zn(ClO_4)_2·6H_2O$: methylsulfonylmethane: H_2O =1.2:3.6:3 (molar ratio)	0.5/0.5	400	98	Adv. Funct. Mater. (2022)[32]
$Zn(TFSI)_2$: diethyl phosphoramidate=1:10 (molar ratio)	0.1/0.1	1200	96	Energy Environ. Sci. (2024)[33]
$Zn(ClO_4)_2·6H_2O$: urethane: H_2O=1:4.5:1 (volume ratio)	1/0.5	700	98.6	Angew. Chem. Int. Ed. (2024)[34]
2 M $ZnSO_4$ + levulinic acid: H_2O=1:1 (volume ratio)	0.5/0.5	300	99.39	Adv. Energy Mater. (2025)[35]
$Zn(OTf)_2$: acetamide:H_2O:DMSO=1:3:24:2 (molar ratio)	1/0.5	1500	99.1	Adv. Mater. (2026)[36]
Choline chloride: N, N-dimethylformamide =1:2 (molar ratio) + 1 M $ZnCl_2$ + 5% AN (volume ratio)	0.5/0.5	400	98.7	J. Am. Chem. Soc. (2025)[37]
$Zn(OTf)_2$: urea: DMSO=1:2:2 (molar ratio)	0.1/0.1	200	98.4	Angew. Chem. Int. Ed. (2026)[38]
$Zn(ClO_4)_2·6H_2O$: $NaClO_4·H_2O$: acetamide=1:1:5 (molar ratio)	0.2/0.2	800	95.5	Angew. Chem. Int. Ed. (2026)[39]
$Zn(BF_4)_2·xH_2O$: acetamide=1:7 + 10% AN (volume ratio)	2/0.5	2000	99.6	This work

References

1. D. Sinnaeve, *Concepts Magn. Reson. Part A*, 2012, **40A**, 39-65.
2. B. D. Adams, J. Zheng, X. Ren, W. Xu and J.-G. Zhang, *Adv. Energy Mater.*, 2018, **8**, 1702097.
3. D. Aurbach, O. Youngman, Y. Gofer and A. Meitav, *Electrochim. Acta*, 1990, **35**, 625-638.
4. K. M. Abraham, Z. Jiang and B. Carroll, *Chem. Mater.*, 1997, **9**, 1978-1988.
5. F. Ciucci, *Curr. Opin. Electrochem.*, 2019, **13**, 132-139.
6. T. H. Wan, M. Saccoccio, C. Chen and F. Ciucci, *Electrochim. Acta*, 2015, **184**, 483-499.
7. F. Ciucci and C. Chen, *Electrochim. Acta*, 2015, **167**, 439-454.
8. J. Hutter, M. Iannuzzi, F. Schiffmann and J. VandeVondele, *Wires Comput. Mol. Sci.*, 2014, **4**, 15-25.
9. B. G. Lippert, J. H. Parrinello and Michele, *Mol. Phys.*, 1997, **92**, 477-488.

10. J. VandeVondele, M. Krack, F. Mohamed, M. Parrinello, T. Chassaing and J. Hutter, *Comput. Phys. Commun.*, 2005, **167**, 103-128.

11. S. Goedecker, M. Teter and J. Hutter, *Phys. Rev. B*, 1996, **54**, 1703-1710.

12. J. P. Perdew, K. Burke and M. Ernzerhof, *Phys. Rev. Lett.*, 1996, **77**, 3865-3868.

13. S. Grimme, J. Antony, S. Ehrlich and H. Krieg, *J. Chem. Phys.*, 2010, **132**, 154104.

14. T. Lu and F. Chen, *J. Comput. Chem.*, 2012, **33**, 580-592.

15. W. Humphrey, A. Dalke and K. Schulten, *J. Mol. Graph.*, 1996, **14**, 33-38.

16. M. Bajdich, M. García-Mota, A. Vojvodic, J. K. Nørskov and A. T. Bell, *J. Am. Chem. Soc.*, 2013, **135**, 13521-13530.

17. H. Bekker, H. Berendsen, E. J. Dijkstra, S. Achterop, R. Drunen, D. van der Spoel, A. Sijbers, H. Keegstra, B. Reitsma and M. K. R. Renardus, *Physics Computing*, 1993, **92**, 252-256.

18. F. Neese, *Wires Comput. Mol. Sci.*, 2012, **2**, 73-78.

19. L. Martínez, R. Andrade, E. G. Birgin and J. M. Martínez, *J. Comput. Chem.*, 2009, **30**, 2157-2164.

20. C. Reichardt, *Chem. Rev.*, 1994, **94**, 2319-2358.

21. X. Lin, G. Zhou, M. J. Robson, J. Yu, S. C. T. Kwok and F. Ciucci, *Adv. Funct. Mater.*, 2022, **32**, 2109322.

22. W. Yang, X. Du, J. Zhao, Z. Chen, J. Li, J. Xie, Y. Zhang, Z. Cui, Q. Kong, Z. Zhao, C. Wang, Q. Zhang and G. Cui, *Joule*, 2020, **4**, 1557-1574.

23. J. Shi, T. Sun, J. Bao, S. Zheng, H. Du, L. Li, X. Yuan, T. Ma and Z. Tao, *Adv. Funct. Mater.*, 2021, **31**, 2102035.

24. R. Chen, C. Zhang, J. Li, Z. Du, F. Guo, W. Zhang, Y. Dai, W. Zong, X. Gao, J. Zhu, Y. Zhao, X. Wang and G. He, *Energy Environ. Sci.*, 2023, **16**, 2540-2549.

25. X. Lu, Z. Liu, A. Amardeep, Z. Wu, L. Tao, K. Qu, H. Sun, Y. Liu and J. Liu, *Angew. Chem. Int. Ed.*, 2023, **62**, e202307475.

26. P. Jaumaux, Q. Liu, D. Zhou, X. Xu, T. Wang, Y. Wang, F. Kang, B. Li and G. Wang, *Angew. Chem. Int. Ed.*, 2020, **59**, 9134-9142.

27. S. Wang, G. Liu, W. Wan, X. Li, J. Li and C. Wang, *Adv. Mater.*, 2024, **36**, 2306546.

28. J. Li, Y. Lou, S. Zhou, Y. Chen, X. Zhao, A. Azizi, S. Lin, L. Fu, C. Han, Z. Su and A. Pan, *Angew. Chem. Int. Ed.*, 2024, **63**, e202406906.

29. H. Qiu, X. Du, J. Zhao, Y. Wang, J. Ju, Z. Chen, Z. Hu, D. Yan, X. Zhou and G. Cui, *Nat. Commun.*, 2019, **10**, 5374.

30. M. Li, X. Wang, J. Hu, J. Zhu, C. Niu, H. Zhang, C. Li, B. Wu, C. Han and L. Mai, *Angew. Chem. Int. Ed.*, 2023, **62**, e202215552.

31. J. Hao, L. Yuan, Y. Zhu, X. Bai, C. Ye, Y. Jiao and S.-Z. Qiao, *Angew. Chem. Int. Ed.*, 2023, **62**, e202310284.

32. M. Han, J. Huang, X. Xie, T. C. Li, J. Huang, S. Liang, J. Zhou and H. J. Fan, *Adv. Funct. Mater.*, 2022, **32**, 2110957.

33. X. Bai, M. Sun, J. Yang, B. Deng, K. Yang, B. Huang, W. Hu and X. Pu, *Energy Environ. Sci.*, 2024, **17**, 7330-7341.

34. M. Qiu, Y. Liang, J. Hong, J. Li, P. Sun and W. Mai, *Angew. Chem. Int. Ed.*, 2024, **63**, e202407012.

35. W. Lv, Y. Tan, C. Guo, X. He, L. Zeng, J. Zhu, L. Yang, Z. Chen, X. Yin, J. Xu and H. He, *Adv. Energy Mater.*, 2025, **15**, 2403689.

36. M. X. Chen, Y. F. Wang, Q. L. Zhang, G. B. Lai, X. Y. Zheng, Y. H. Zhuang, Z. H. Du, K. L. Xia, L. Y. Li, J. Q. Weng, Z. X. Lu, F. Liu, Z. Y. Liu, C. K. Yang, W. Liu, M. M. Wu and Z. G. Zou, *Adv. Mater.*, 2026, **38**, e08315.

37. X. Zhang, Q. Tang, H. Luo, Y. Xu, S. Miao, S. Zhou, C. Xu, Y. Jia, Q. He, J. Peng, L. He, Y. Song, Y. Zhang and W. Cai, *J. Am. Chem. Soc.*, 2025, **147**, 39440-39451.

38. J. Yan, X. Zhao, J. Feng, Z. Li, Z. Bai, X. Hou, H. Li, H. Wei and S. Dou, *Angew. Chem. Int. Ed.*, 2026, **65**, e14392.

39. M. Y. Zhu, W. J. Cheng, H. B. Wang, C. X. Li, H. C. Wang, J. Yang, Y. J. Chen, S. Li, H. Wu, S. Chen, T. Y. Gao, Y. X. Tang and Y. Y. Zhang, *Angew Chem Int Edit*, 2026, DOI: 10.1002/anie.202518700, e18700.